Theoretical model for the performance of a multi-spectral imaging sensor

Xiaorui Wang (王晓蕊)*, Honggang Bai (白宏刚), and Jianqi Zhang (张建奇)

School of Technical Physics, Xidian University, Xi'an 710071, China

**E-mail: xrwang@mail.xidian.edu.cn*

Received May 11, 2009

A new performance metric, the two-dimensional (2D) contrast threshold surface, is proposed to characterize the systematic performance of a multi-spectral imaging sensor. Specifically, how to measure this performance metric is presented based on the discriminations of a set of sine-wave test patterns with different radiance magnitudes and spectral properties. The theoretical model for predicting the 2D contrast threshold surface is derived based on an analytical description of the effective contrast between the test pattern and its background, in which the impacts of fusion algorithms on the 2D contrast threshold surface are also discussed using the minimum threshold match criteria. Preliminary simulation results show that this model can be used to quantitatively characterize the real influence of the spectral differences and spatial frequencies on the contrast thresholds required for the observer to just resolve the images of the test patterns through a multi-spectral imaging sensor.

OCIS codes: 110.0110, 110.4234, 110.3000.

doi: 10.3788/COL20100802.0155.

Over the past decades, multi-spectral imaging sensors have experienced rapid development. Basically, multi-spectral imaging sensors have two or more channels that are sensitive in different spectral regions, which promise significant improvements in the target acquisition (TA) performance. With this type of imaging sensor, targets may be distinguished from their backgrounds not only on the basis of differences in radiation magnitude in the sensor's spectral range differences (as the case with single-band imaging sensors), but also on differences in spectral properties. However, current existing end-to-end sensor performance measures, such as the minimum resolvable temperature difference (MRTD)[1] or the minimum resolvable contrast (MRC), the minimum temperature difference perceived (MTDP)[2], the triangle orientation discrimination (TOD) threshold laboratory test[3−5], and NVThermIP[6] model, produce threshold curves of resolution versus the thermal or luminance contrast and do not take the spectral difference into account. To overcome the shortcoming of current performance methods for characterizing a multi-spectral imaging sensor, some researchers have made attempts. Piet *et al*. proposed an extension to the current TOD test methods, which yields a two-dimensional (2D) TOD surface of the resolution, contrast, and spectral difference between a triangle test pattern and its background[7]. But no further effort was made to study its theoretical model due to the complex analytical description of the triangle pattern. Another research perspective is to quantitatively assess multi-spectral image quality by introducing some figure of merits, such as analysts' interpretation of quality and utility[8], spectral similarity[9], and spectral quality equation[10]. However, these metrics are only appropriate for the detection task of an unresolved object, not considering the target recognition and identification tasks of an extended source target. To compare two competing multi-spectral imaging sensors, or to quantify the anticipated benefits of a multi-spectral imaging sensor above a single-band imaging system, we propose a 2D contrast threshold surface for characterizing a multi-spectral imaging sensor, and derive its theoretical model based on the perceptual property of the human visual system (HVS). Moreover, the impacts of image fusion algorithms on this performance metric are investigated. Simulation results show that this performance theoretical model can correctly predict the quantitative trade-off relationship among the spectral differences, the radiance differences, and the spatial frequencies for particular TA task.

For a single-band imaging sensor based on human vision, the widely used performance metrics such as MRTD or MRC are generally measured through a blackbody source or a single color for the test pattern and background, which can be closely related to the TA performance through John criteria[11]. However, the performance metrics similar to MRTD or MRC have not been studied for multi-spectral imaging sensors based on human vision. Different from single-band imaging sensors, the TA performance is not only due to the spatial size and luminance contrast of the target, but also dependent on the spectral difference between the target and its backgrounds in certain scenarios (for TA purposes, e.g., trees, grass, concrete, low emissive paint, camouflage nets). Therefore, how to correctly configure the spectral differences, radiance differences, and spatial frequencies of the test patterns and its backgrounds is the prerequisite to measure the systematic performance metrics related to its TA performance. On the other hand, the fused gray images from different channels are eventually observed by the HVS. The contrast sensitivity function of HVS directly determines the required contrast threshold for the observer to discriminate the test pattern images through a multi-spectral imaging sensor. Moreover, the experimental study of the contrast sensitivity function of HVS is generally based on a set of sine-wave patterns from the perception perspective[12]. Hence, to measure the proposed performance metric, we choose multiple sets of sine-wave patterns with adjustable radiance differences,

spectral differences, and different spatial frequencies as the test patterns. Specific procedures are given as follows.

1) It is first assumed that a multi-spectral imaging sensor is generally used in a certain field background with a luminance of L_{B} and a spectral reflectivity of $\rho_{\mathrm{B}}(\lambda)$. The maximum spectral reflectivity of real target sensed in this natural scene is supposed to be $\rho_{\mathrm{T}}(\lambda)$.

2) To measure the performance metric related to the TA performance, the test pattern background is configured to be the same as the field background in the luminance and spectral reflectivity, also expressed by L_{B} and $\rho_{\mathrm{B}}(\lambda)$, respectively. The luminance of the test pattern is represented by L_{T}.

3) Considering the relevant combinations of different type of real targets and field backgrounds in natural scene, we define the reflectivity of the test pattern as

$$\rho_{\mathrm{Bar}}(\lambda) = \alpha\left(\rho_{\mathrm{T}}(\lambda) - \rho_{\mathrm{B}}(\lambda)\right) + \rho_{\mathrm{B}}(\lambda), \tag{1}$$

where α is the spectral difference coefficient, which is an additional variable. If α=1, the test pattern spectral properties equal those of the selected target. If α=0, the spectral reflectivities of the test pattern and background are equal, yielding a test very similar to the standard performance test for a single-band imaging sensor. Now, instead of varying the test pattern size and luminance only, also the spectral reflectivity of the test pattern can be varied in the performance metric measurement.

4) The luminance and reflectivity of the test pattern background is kept constant. We suppose that the images from different spectral channels are displayed in gray. The measurement procedure similar to MRC is adopted. The correct fraction of the HVS as a function of test pattern contrast for a range of test pattern spatial frequencies and a range of values of α. If possible, we determine the contrast threshold at 50% correct response probability. If, for certain spatial frequency and α, the correct fraction does not fall below 50%, the test pattern can be detected on the basis of reflectivity difference and contrast being equal to zero.

5) Finally, construct a perceptual 2D contrast threshold surface in the three-dimensional (3D) space with the spatial frequency, contrast, and α as ordinates.

According to the above descriptions, we know that this perceptual 2D contrast threshold surface is obtained based on the perceptual properties of the HVS to the gray images of a set of test sine-wave patterns through a multi-spectral imaging sensor. Hence, it is necessary to combine the optical properties of sine-wave test patterns, their transfer properties through a multi-spectral imaging sensor, and the contrast sensitivity of the HVS to establish a theoretical model for predicting the new performance metric. Considering the test patterns being the input signal of a multi-spectral imaging sensor, we need to start with a mathematical description of the test pattern. Note that the optical properties of the test patterns are adjusted by changing the luminance and the spectral reflectivity of the test pattern and its background. Then, the effective contrast of the test pattern and its background can be expressed as

$$C_{\mathrm{eff}} = \frac{\rho_{\mathrm{Bar}}(\lambda) L_{\mathrm{T}} - \rho_{\mathrm{B}}(\lambda) L_{\mathrm{B}}}{\rho_{\mathrm{Bar}}(\lambda) L_{\mathrm{T}} + \rho_{\mathrm{B}}(\lambda) L_{\mathrm{B}}}. \tag{2}$$

Substituting Eq. (1) into Eq. (2), we can get

$$C_{\mathrm{eff}} = \frac{\left[\alpha\left(\rho_{\mathrm{T}}(\lambda) - \rho_{\mathrm{B}}(\lambda)\right) + \rho_{\mathrm{B}}(\lambda)\right] L_{\mathrm{T}} - \rho_{\mathrm{B}}(\lambda) L_{\mathrm{B}}}{\left[\alpha\left(\rho_{\mathrm{T}}(\lambda) - \rho_{\mathrm{B}}(\lambda)\right) + \rho_{\mathrm{B}}(\lambda)\right] L_{\mathrm{T}} + \rho_{\mathrm{B}}(\lambda) L_{\mathrm{B}}}. \tag{3}$$

Equation (3) is further expressed as

$$C_{\mathrm{eff}} = \frac{\left[\alpha\left(\rho_{\mathrm{T}}(\lambda) - \rho_{\mathrm{B}}(\lambda)\right) + \rho_{\mathrm{B}}(\lambda)\right]\left(L_{\mathrm{B}} + \Delta L\right) - \rho_{\mathrm{B}}(\lambda) L_{\mathrm{B}}}{\left[\alpha\left(\rho_{\mathrm{T}}(\lambda) - \rho_{\mathrm{B}}(\lambda)\right) + \rho_{\mathrm{B}}(\lambda)\right]\left(\mathrm{L}_{\mathrm{B}} + \Delta L\right) + \rho_{\mathrm{B}}(\lambda) L_{\mathrm{B}}}, \tag{4}$$

where ΔL is the difference between the test pattern luminance L_{T} and its background luminance L_{B}. With both the numerator and denominator in the right part of Eq. (4) being divided by L_{B}, we can obtain

$$C_{\mathrm{eff}} = \frac{\left[\alpha\left(\rho_{\mathrm{T}}(\lambda) - \rho_{\mathrm{B}}(\lambda)\right) + \rho_{\mathrm{B}}(\lambda)\right](1 + C) - \rho_{\mathrm{B}}(\lambda)}{\left[\alpha\left(\rho_{\mathrm{T}}(\lambda) - \rho_{\mathrm{B}}(\lambda)\right) + \rho_{\mathrm{B}}(\lambda)\right](1 + C) + \rho_{\mathrm{B}}(\lambda)}, \tag{5}$$

where C is the ratio of ΔL to L_{B}, representing the controllable luminance contrast of the test pattern and its background in the performance measurement procedure.

Now, we need to consider the transfer properties through each imaging channel of the sine-wave test pattern. According to the linear system theory, the contrast of the output image of the sine-wave patterns thought each imaging channel is written as

$$C^n_{\mathrm{out-eff}} = C_{\mathrm{eff}} \cdot H^n_{\mathrm{sys}}(\xi), \tag{6}$$

where $H^n_{\mathrm{sys}}(\xi)$ is the system modulation transfer function (MTF) of the nth imaging channel (including optics, detector, and display MTFs). Since the perceptual 2D contrast threshold surface is defined as the input optical properties required for the HVS to just resolve the images of the test pattern, we need to further obtain the perceptual contrast of the HVS to the test pattern images. Additionally, noise characteristic also has significant effects on the perceptual contrast of the output image of the test pattern, which should be taken into account. Equation (6) can be then modified as the perceptual image contrast considering the perceived properties of the HVS to the test pattern images including noise[13]:

$$C^n_{\mathrm{perceptual}} = C^n_{\mathrm{out-eff}} \Big/ \left(1 + \frac{\kappa^2 \mathrm{PSD}^n \cdot Q^n_{\mathrm{h}}(\xi) Q^n_{\mathrm{v}}}{L^2}\right)^{1/2}, \tag{7}$$

where κ is the calibration constant; PSD^n represents the detector noise power spectral density of the nth imaging channel in units of $\mathrm{fL}^2{\cdot}\mathrm{s}{\cdot}\mathrm{mrad}^2$; Q^n_{h} is the horizontal noise bandwidth of the nth imaging channel[13], which is related to post-filter MTFs from electronics, display, and the eye and the bandpass properties of the HVS; Q^n_{v} is the vertical noise bandwidth of the nth imaging channel[13], which is related to post-filter MTFs from electronics, display, and the eye; L is the display luminance in fL.

For an observer to just be able to resolve an input test pattern, the output contrast modulation in Eq. (7) should be equal to or higher than the contrast modulation threshold of the human visual system. Barten established a theoretical model $\mathrm{CTF}_{\mathrm{eye}}(\xi)$of contrast threshold function corresponding to 50% correct response probability of the observer by using the experimental data collected by psychophysicists[12]. To achieve the 2D contrast

threshold surface, we set the perceptual image contrast of the test pattern, $C^n_{\text{perceptual}}$, to be equal to the contrast threshold function $\text{CTF}_{\text{eye}}(\xi)$ of the human eye, and consider the conversion of the unit of the spatial frequency from the image space to the visual space. We can get

$$C^n_{\text{perceptual}} = \text{CTF}_{\text{eye}}(\xi/m), \tag{8}$$

where m is the angular magnification factor of each imaging channel.

Combining Eqs. (5)–(8), we can get the input contrast thresholds required for the observer just being able to discriminate the test pattern images after some conversions:

$$\text{CT}^n_{\text{input}} = \frac{\text{CTF}^n_{\text{sys}}(\xi)\left[\alpha\left(\rho_{\text{T}}(\lambda) - \rho_{\text{B}}(\lambda)\right) + 2\rho_{\text{B}}(\lambda)\right] - \alpha\left(\rho_{\text{T}}(\lambda) - \rho_{\text{B}}(\lambda)\right)}{\left(1 - \text{CTF}^{\text{n}}_{\text{sys}}(\xi)\right)\left[\alpha\left(\rho_{\text{T}}(\lambda) - \rho_{\text{B}}(\lambda)\right) + \rho_{\text{B}}(\lambda)\right]},$$

where

$$\text{CTF}^n_{\text{sys}}(\xi) = \frac{\text{CTF}_{\text{eye}}(\xi/m)}{H^n_{\text{sys}}(\xi)} \cdot \left(1 + \frac{\kappa^2 \text{PSD}^n \cdot Q^n_{\text{h}}(\xi) Q^n_{\text{v}}}{L^2}\right)^{1/2}. \tag{9}$$

From Eq. (9), it can be seen that this contrast threshold is a 2D function of the spectral difference coefficient and spatial frequency.

It is known that the main purpose of fusion algorithms is to extract complementary image information and combine similar image information from each channel, and then form the optimum image information for the observer. Here, the contribution of fusion algorithms to the integral performance is taken as an optimum threshold matched filter, i.e.,

$$\text{CT}_{\text{fusion}} = \min \left\{\text{CT}^1_{\text{input}}, \text{CT}^2_{\text{input}}, \cdots, \text{CT}^n_{\text{input}}, \cdots, \text{CT}^N_{\text{input}}\right\}, \tag{10}$$

where $\text{CT}^1_{\text{input}}$, $\text{CT}^2_{\text{input}}$,$\cdots$, $\text{CT}^N_{\text{input}}$ are the input contrast thresholds required corresponding to various imaging channels included in a multi-spectral imaging sensor, respectively. In principle, Eq. (10) can provide the optimum thresholds through a comparison of different imaging channel thresholds corresponding to the same spatial frequency and spectral difference, which can objectively reflect the action of fusion algorithms.

Next, we use the performance theoretical model to perform a simulation focusing on a multi-spectral imaging sensor with three spectral imaging channels. It is assumed that the total MTFs (including optics, detector, and display MTFs) of three imaging channels are, respectively,

$$H^1_{\text{sys}}(\xi) = \text{e}^{-0.07\xi^2}, \quad H^2_{\text{sys}}(\xi) = \text{e}^{-0.09\xi^2}, \quad H^3_{\text{sys}}(\xi) = \text{e}^{-0.05\xi^2}, \tag{11}$$

where ξ is the spatial frequency in cycle/mrad. The corresponding post-filter MTFs are, respectively,

$$H^1_{\text{post}}(\xi) = \text{e}^{-0.035\xi^2}, \quad H^2_{\text{post}}(\xi) = \text{e}^{-0.05\xi^2}, \quad H^3_{\text{post}}(\xi) = \text{e}^{-0.025\xi^2}. \tag{12}$$

We suppose that their signal-to-noise ratios (SNRs) for the average pixel are 8:1, 10:1, and 12:1, respectively. The PSD is the square of the root-mean-square (RMS) noise for 1 s and 1 mrad in each dimension. All of these three display signal luminances are 5 fL. Their system magnification factors are the same, equal to 10.

Based on the above parameters, the simulated results are obtained, as shown in Figs. 1–4. Figures 1–3 show the contrast threshold surfaces of three different spectral imaging channels, respectively. Each contrast threshold surface is affected by both the spatial frequency and the spectral difference of the test pattern and its background. As the spatial frequency increases, the required contrast thresholds become larger gradually for the observer to just resolve the test pattern with particular spectral difference. The contrast threshold values are relatively smaller for larger spectral difference coefficients. We also find that the needed contrast thresholds are higher for the target patterns of lower spatial frequencies compared with those of medium spatial frequencies, which is due to the inhibitory signal processing

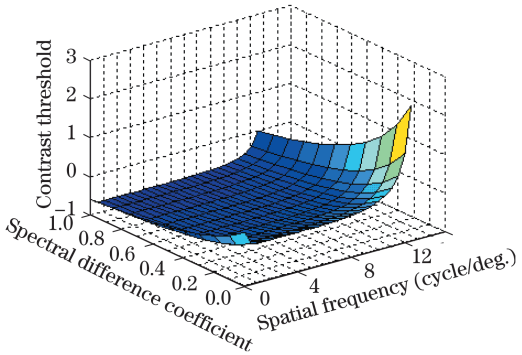

Fig. 1. Contrast threshold surface for channel 1.

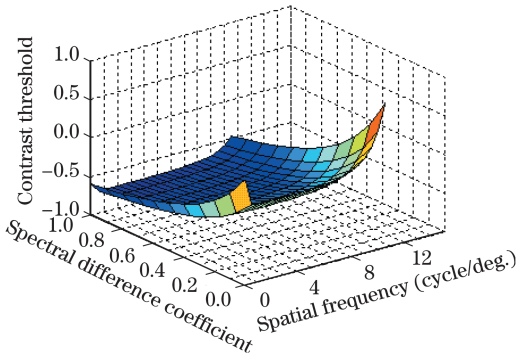

Fig. 2. Contrast threshold surface for channel 2.

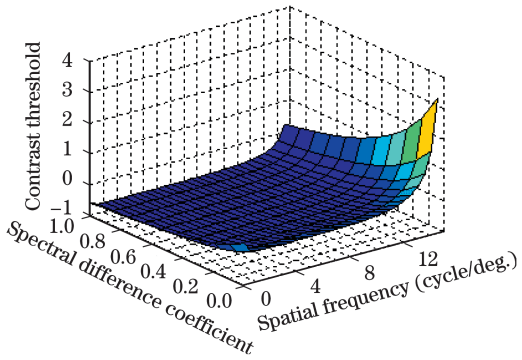

Fig. 3. Contrast threshold surface for channel 3.

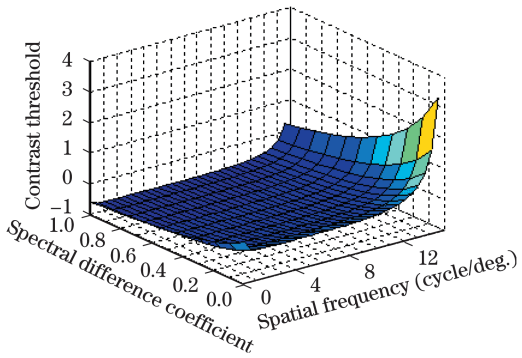

Fig. 4. Contrast threshold surface for a multi-spectral imaging sensor.

of the HVS. On the other hand, it can be seen that some values of contrast thresholds are negative, which means that the luminance values of the needed test pattern are possibly lower than that of its background when the spectral reflectivity of the test pattern is much larger than that of its background. Summarily, the interrelationships of these three physical factors are consistent to the sensing phenomenon of a multi-spectral imaging sensor in real TA task, which means that the same trade-off relationship among the spectral difference, contrast, and spatial frequency of real target and field background exists for particular TA task. Although they show the same change trend, these threshold surfaces also have significant differences in the contrast threshold range due to the differences of channel design parameters. Figure 4 shows the most sensitive contrast threshold surface of a multi-spectral imaging sensor after fusion of the above three imaging channels, which can reflect the complementary information of each channel and form the most optimum threshold surface required to discriminate the test pattern. This point is consistent with the conclusion drawn in Ref. [7].

In conclusion, a 2D contrast threshold surface for evaluating the systematic performance of a multi-spectral imaging sensor is proposed. How to define the spectral property of the test pattern is deeply discussed for measuring the 2D contrast threshold surface. The theoretical model of the 2D contrast threshold surface is derived on the basis of the perceptual property of the HVS, in which the contributions of fusion algorithms are quantitatively described. Simulation results show that this model can not only be related to imaging properties of each channel included in a multi-spectral imaging sensor, but also combine the improvement of fusion algorithms to the total performance. This performance metric may be a promise method to optimize the design parameters of a multi-spectral imaging sensor and for fusion algorithm developments from the system-level performance perspective. In the near future, we will explore to predict the TA task performance of multi-spectral imaging sensors based on this theoretical model.

This work was supported by the Key Project of Ministry of Education of China (No. 109143), Research Funds for the Doctoral Program of Higher Education (No. 20070701020), and the Aviation Science Funding (No. 20070181005).

References

1. R. G. Driggers, V. Hodgkin, R. H. Vollmerhausen, and O. S. Patrick, Proc. SPIE **5076,** 179 (2003).
2. W. Wittenstein, Opt. Eng. **38,** 773 (1999).
3. P. Bijl and J. M. Valeton, Proc. SPIE **3377,** 182 (1998).
4. X. Wang, J. Zhang, Z. Feng, and H. Chang, Acta Opt. Sin. (in Chinese) **25,** 1036 (2005).
5. J. Wang, W. Jin, L. Wang, Y. He, and X. Wang. Acta Opt. Sin. (in Chinese) **28,** 2125 (2008).
6. R. H. Vollmerhausen, E. Jacobs, and R. G. Driggers, Opt. Eng. **43,** 2806 (2004).
7. B. Piet and A. H. Maarten, Proc. SPIE **5076,** 208 (2003).
8. P. K. John, W. M. David, L. Pau, and E. S. Rulon, Proc. SPIE **6230,** 62330W (2006).
9. P. K. John, P. C. Adam, and E. S. Rulon, Proc. SPIE **5806,** 469 (2005).
10. E. S. Rulon, D. E. Timothy, and J. S. David, Proc. SPIE **5806,** 457 (2005).
11. X. Wang, W. Xie, H. Chang, and J. Zhang. Int. J. Infrared Millimeter Waves **26,** 1031 (2005).
12. P. Barten, SID 92 Digest 867 (1992).
13. J. Eddie, R. G. Driggers, and R. H. Vollmerhausen, Proc. SPIE **5612,** 284 (2004).